Geochemical evidence for high volatile fluxes from the mantle at the end of the Archaean

Bernard Marty, David V. Bekaert, Michael W. Broadley, Claude Jaupart

Geochemical evidence for high volatile fluxes from the mantle at the end of the Archaean

Bernard Marty[1]*, David V. Bekaert[1], Michael W. Broadley[1] & Claude Jaupart[2]

The exchange of volatile species—water, carbon dioxide, nitrogen and halogens—between the mantle and the surface of the Earth has been a key driver of environmental changes throughout Earth's history. Degassing of the mantle requires partial melting and is therefore linked to mantle convection, whose regime and vigour in the Earth's distant past remain poorly constrained[1,2]. Here we present direct geochemical constraints on the flux of volatiles from the mantle. Atmospheric xenon has a monoisotopic excess of ^{129}Xe, produced by the decay of extinct ^{129}I. This excess was mainly acquired during Earth's formation and early evolution[3], but mantle degassing has also contributed ^{129}Xe to the atmosphere through geological time. Atmospheric xenon trapped in samples from the Archaean eon shows a slight depletion of ^{129}Xe relative to the modern composition[4,5], which tends to disappear in more recent samples[5,6]. To reconcile this deficit in the Archaean atmosphere by mantle degassing would require the degassing rate of Earth at the end of the Archaean to be at least one order of magnitude higher than today. We demonstrate that such an intense activity could not have occurred within a plate tectonics regime. The most likely scenario is a relatively short (about 300 million years) burst of mantle activity at the end of the Archaean (around 2.5 billion years ago). This lends credence to models advocating a magmatic origin for drastic environmental changes during the Neoarchaean era, such as the Great Oxidation Event.

The terrestrial atmosphere contains a ^{129}Xe monoisotopic excess of 7.3% relative to primordial (solar or meteoritic) xenon, attributed[7] to the decay of the extinct radioisotope ^{129}I. Some ^{129}Xe may also have been inherited from comets during the early stages of Earth's accretion[3]. Atmospheric xenon evolved subsequently through mass-dependent fractionation (MDF) due to selective atmospheric escape[4,5,8,9], while preserving the mass-independent, monoisotopic excess of ^{129}Xe. Degassing of mantle xenon through volcanism contributed further ^{129}Xe to the atmospheric inventory, because mantle xenon is enriched in ^{129}Xe. (Values of ^{129}Xe/^{130}Xe up to 7.0 are found for mantle plumes, and up to 7.8 for mid-ocean ridge basalt (MORB) mantle source[10,11], relative to the present-day atmospheric Xe signature[7], ^{129}Xe/^{130}Xe = 6.496). Remnants of ancient atmospheric gases have been identified in fluid inclusions hosted in Archaean hydrothermal quartz[5,8,9,12] and trapped in organic matter isolated from Archaean chert[4], all from Australia and South Africa. Whereas nitrogen, neon, argon (^{36}Ar, ^{38}Ar) and krypton have isotopic compositions indistinguishable from the modern atmospheric values[4,5,8,12], xenon isotopes are subject to MDF to an extent that is intermediate between the composition of the atmospheric Xe ancestor (labelled U-Xe) and the modern composition. The extent of isotope fractionation increased with time to reach the modern Xe composition[5] around 2 billion years ago (Ga). Together with the under-abundance of Xe in air relative to the expected abundance pattern of chondritic noble gases, this evolution has been attributed to selective Xe escape from the atmosphere to space via a non-thermal escape process related to interactions between the upper atmosphere's atoms and ultraviolet photons from the young Sun[5,13].

Samples with ages between 3.3 Ga and 2.7 Ga present comparable depletions of ^{129}Xe relative to adjacent ^{128}Xe and ^{130}Xe isotopes irrespective of their sampling location, whereas more recent samples have compositions consistent with that of modern atmospheric Xe (Figs. 1 and 2; Extended Data Table 1). The deficit of ^{129}Xe in the Archaean atmosphere (denoted $^{129}Xe_{DEF}$) was compensated over time by degassing of ^{129}Xe-rich mantle xenon (labelled $^{129}Xe_{XS}$, where suffix XS refers to ^{129}Xe in excess of the atmospheric composition: $^{129}Xe_{XS} = {}^{130}Xe_{mantle} \times \{(^{129}Xe/^{130}Xe)_{mantle} - (^{129}Xe/^{130}Xe)_{atm}\}$). We define Δ^{129}Xe as the deviation of the sample ^{129}Xe/^{130}Xe from the value expected for fractionated modern atmospheric xenon, in parts per thousand (‰) (Fig. 1). All available data[4–6,8] define a clear evolution from negative Δ^{129}Xe values around 3 Ga trending towards a modern-like composition starting around 2 Ga (Figs. 2 and 3). This evolution suggests that the flux of $^{129}Xe_{XS}$ from the mantle has varied considerably over time.

The amount of $^{129}Xe_{DEF}$ 3.3–2.7 Ga ago was $(2.56 \pm 1.02) \times 10^{10}$ mol (95% confidence intervals, CI), computed with an error-weighted average

[1]Centre de Recherches Pétrographiques et Géochimiques, UMR 7358 CNRS and Université de Lorraine, Vandoeuvre-les-Nancy, France. [2]Université de Paris, Institut de Physique du Globe de Paris, CNRS, Paris, France. *e-mail: bernard.marty@univ-lorraine.fr

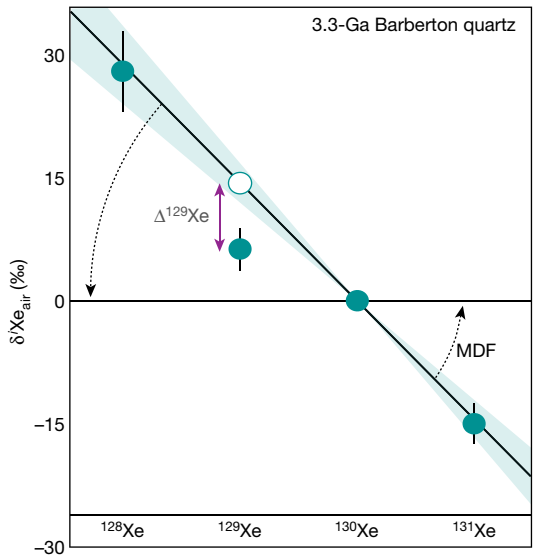

Fig. 1 | Principle of xenon isotope evolution over time. Data (filled symbols, error bars are 1σ) for fluid inclusions in 3.3-Ga Barberton (South Africa) hydrothermal quartz[8] exemplify the Xe isotope composition of Archaean air, normalized to the composition of modern air (horizontal black line). The Xe isotopic composition of the Archaean atmosphere is mass-dependently fractionated, being enriched in light isotopes relative to heavy ones. The measured ^{129}Xe/^{130}Xe ratio is, however, below the isotope fractionation line defined by the other Xe isotopes. This depletion in ^{129}Xe/^{130}Xe, denoted Δ^{129}Xe, is defined as the distance between the observed value and that expected for isotope fractionation of modern air (open symbol). The dotted arrows indicate the evolution of Xe isotope fractionation through time, yielding the modern composition around 2 Ga. The light green shading around the isotope fractionation line represents the 2σ error of the error-weighted linear correlation through Xe isotope data, excluding ^{129}Xe.

Δ^{129}Xe of (−6.3 ± 2.5)‰ (Barberton, MGTKS3#2 and Fortescue samples, Extended Data Table 1; 95% CI)). The fractionation of Xe isotopes in the ancient atmosphere strongly suggests[4,5,8,9,13] that a large fraction of xenon was lost to space between 3 Ga and 2 Ga. Considering either an exponential law[9] or a power law[4] for Xe escape results in essentially the same loss of atmospheric xenon, equivalent to 2.5 ± 0.5 times the modern atmospheric Xe inventory (Extended Data Fig. 1). By incorporating the simultaneous loss of atmospheric xenon to space during the Archaean, the total amount of ^{129}Xe$_{DEF}$ could have been as high as (8.96 ± 3.57) × 10^{10} mol (Extended Data Table 2).

Delivery of cometary Xe is an unlikely process to account for the temporal evolution of atmospheric Δ^{129}Xe (Methods), and we consider volcanic degassing of ^{129}Xe$_{XS}$ as the main source of Δ^{129}Xe variation. Contrary to the case of radiogenic ^{40}Ar, which was degassed from both the mantle and the continental crust through time[14], a mantle-only origin for radiogenic ^{129}Xe is certain, so that accumulation in the atmosphere directly traces time-dependent mantle degassing and convection. Since about 3 Ga, the average flux of ^{129}Xe$_{XS}$ from the mantle to the atmosphere necessary to compensate for ^{129}Xe$_{DEF}$ in the Archaean atmosphere is equivalent to 8.5 ± 3.4 mol yr^{-1} (closed system atmosphere[8]), or 30 ± 12 mol yr^{-1} (taking into account xenon lost to space) (95% CI). We estimate the modern flux of ^{129}Xe$_{XS}$ independently by scaling the Xe/He ratio measured within mantle-derived samples to the ^{3}He mantle flux in the oceans from submarine volcanism[15], and from subaerial volcanoes[16] to be 0.9 ± 0.5 mol yr^{-1} (Methods; Extended Data Table 2). Thus modern degassing rate averaged over 3 Ga would fail by one order of magnitude to supply the amount of ^{129}Xe$_{DEF}$ that was missing in the Archaean atmosphere.

We modelled the evolution of atmospheric Xe through time by MDF[4] with different functions estimating the evolution of Δ^{129}Xe (Fig. 2A–D; Methods). The model considers both cases of a closed system atmosphere and progressive escape to space, with, in the latter case, the amount of lost Xe (2.5 times the modern Xe inventory in total) being scaled to the isotopic evolution of atmospheric Xe (Methods, Extended Data Fig. 1). This model is iterative, combining progressive loss and MDF fractionation of atmospheric xenon until 2.0 Ga with the time-dependent evolution of Δ^{129}Xe (Extended Data Fig. 1). The model requires the ^{129}Xe/^{130}Xe ratio of the ancient mantle to be estimated. Because the production of substantial amounts of radiogenic ^{129}Xe would have occurred only during the first 100 million years (Myr) of Earth's history given the half-life of parent ^{129}I (15.7 Myr), the ^{129}Xe/^{130}Xe ratio could have only evolved by subduction/recycling of 'modern-like' atmospheric xenon into the mantle[8,11,17]. From mass balance, we estimate that the pre-subduction ^{129}Xe/^{130}Xe ratio of the mantle was in the range 14 ± 1 (Methods; Extended Data Fig. 2). Although the recycling history of atmospheric Xe into the mantle between 3 Ga and 1 Ga is not known, numerical modelling of Xe evolution in the mantle–atmosphere system suggests that the imprint of recycling became quantitatively important only from 1 Ga (Extended Data Fig. 3, ref. [17]). To circumvent this uncertainty, we modelled the evolution of Δ^{129}Xe in the time interval 3–1 Ga. The evolution of Δ^{129}Xe is then modelled assuming that mantle degassing decreased continuously (using exponential and power laws) since the Archaean (Fig. 2A–C). Both exponential and power laws give similar outcomes for the flux of mantle-derived ^{129}Xe to the 3-Ga atmosphere, 18 mol yr^{-1} and 63 mol yr^{-1}, respectively, without considering escape, and 64 mol yr^{-1} and 220 mol yr^{-1}, respectively, if loss to space is taken into account.

However, near-constant Δ^{129}Xe in the range 3.3–2.7 Ga followed by a stepwise change to the modern value around 2.6–2.0 Ga (Fig. 2d) strongly suggest that the Neoarchaean was punctuated by a short burst of intense magmatic activity, consistent with the evolution of mantle potential temperatures through time[18] (Fig. 3). For such a model, considering a distinct period of intense degassing between 2.6 Ga and 2.2 Ga, we calculate a peak degassing rate of 141 mol yr^{-1} for escape to space (Extended Data Table 4). For comparison, we estimate the modern flux of mantle-derived ^{129}Xe to be 6.3 ± 2.6 mol yr^{-1} (computed with a ^{130}Xe flux of 0.85 ± 0.35 mol yr^{-1}, Extended Data Table 2, and an average mantle ^{129}Xe/^{130}Xe ratio of 7.4 ± 0.4). Our estimates rely on the mantle ^{129}Xe/^{130}Xe ratio, which is taken here to be maximal at 14 (corresponding to a pre-subduction signature; Methods). If this ratio were to be lower in the ancient mantle owing to an early onset of subduction (down to potential modern values of 7–8), then our estimates of mantle Xe fluxes would be increased substantially, by up to one order of magnitude (Extended Data Fig. 6). We therefore consider our degassing rate estimates reported above to represent lower limits. Irrespective of the model chosen, it is therefore clear that substantially higher mantle fluxes are required in the Archaean. Enhanced degassing would have had a marginal effect on the atmospheric ^{40}Ar/^{36}Ar ratio (Methods; Extended Data Fig. 4) and would be difficult to detect in other Xe isotope ratios of Archaean samples (for example, the fissiogenic ones) because all Archaean samples contain an inherited or produced fissiogenic excess that is likely to mask the original atmospheric composition (Methods).

Given the incompatibility of xenon during partial melting[19], the rate of mantle degassing is related to mantle melting. However, higher concentrations of Xe in the Archaean mantle relative to its present-day budget could potentially lower the amount of mantle degassing necessary to account for the evolution of the ^{129}Xe deficit in the Archaean atmosphere. Indeed, models investigating the time evolution of the ^{3}He/^{4}He ratio of the mantle, for example, suggest mantle ^{3}He concentrations to be higher during the Archaean[20]. With our numerical simulations (Fig. 2), we estimate that 3%–39% of xenon could have been degassed from the mantle since the Archaean, irrespective of the model adopted (Extended Data Table 4). From estimates of the present-day Xe content of the mantle calculated from the ^{130}Xe/^{3}He ratio and the modern

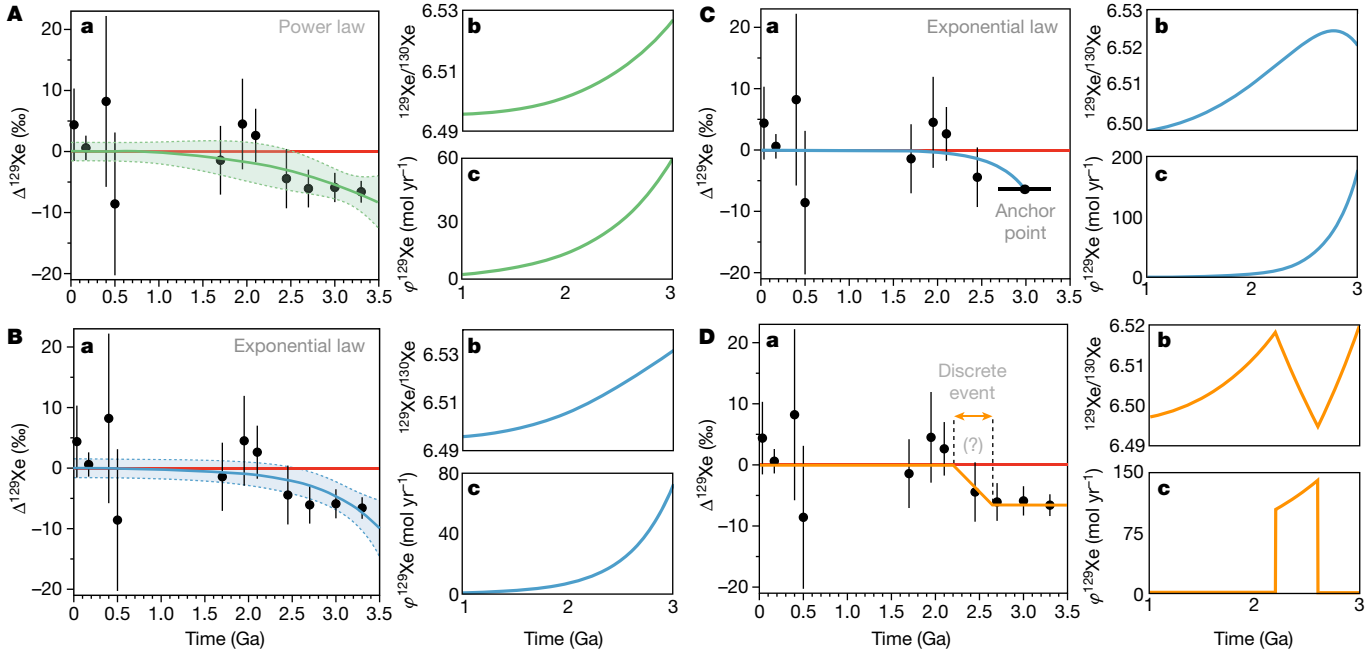

Fig. 2 | Time evolution of the deficit of ^{129}Xe (Δ^{129}Xe) in ancient atmospheric gases, of the atmospheric ^{129}Xe/^{130}Xe ratio, and of the flux of ^{129}Xe from the mantle (ϕ^{129}Xe). Data and references are given in Extended Data Table 1. The data are modelled in four ways: using power (**A**) and exponential (**B**) laws fitted through all data points; using an exponential law fitted through an anchor point at 3 Ga, −6.3‰ (**C**); and using a ramp function used to mimic the effect of a massive, discrete episode of degassing 2.6–2.2 Ga (**D**). For each of the four models **A**–**D** are shown three plots: **a**, Δ^{129}Xe versus time (data points), with a curve fitted to the data; **b**, ^{129}Xe/^{130}Xe versus time; and **c**, ϕ^{129}Xe versus time. In the plots of Δ^{129}Xe, the curves and error areas (**A**,**a**, **B**,**a**; 95% confidence interval) were produced using the error-weighted solver function of the Matlab curve-fitting tool.

^{3}He-degassing rate, we also find that the Archaean mantle Xe content could have been at best a factor of 2 higher than that of the modern mantle (Methods, Extended Data Table 2). Moderate mantle noble-gas depletion since the Archaean is independently indicated by Ne isotope systematics of the mantle–atmosphere system (Methods). We conclude that higher noble-gas concentrations in the ancient mantle cannot account for the ≥10 times greater Xe mantle fluxes in the distant past, thus calling for enhanced magma production rates in the Neoarchaean.

We evaluate here which scenario—continuous decrease in mantle degassing with time or a short-lived burst of activity in the 2.6–2.2 Ga time period—is most likely within the framework of past mantle dynamics. The former model represents the secular waning of melt generation at mid-ocean ridges and can in principle be rejected, as we now explain. In the Neoarchaean, ambient mantle temperatures were higher than today, implying larger melt fractions[18,21,22], but melt production rates depend on plate velocities, which are poorly constrained for that time. Extending plate tectonics models far back in time is fraught with severe uncertainties[18,21,22]. The global rate of plate renewal, however, is directly related to the Earth's heat loss, which can be deduced from changes of the ambient mantle temperature through time. Going back in time, this temperature increases and peaks at about 1,600 °C at an age in the 2.5–3.0 Ga range[18] (Fig. 3). Data for greater ages up to 3.5 Ga do not indicate any further temperature variation[18]. Thus, by definition, the mantle cooling rate was effectively zero at about 2.5 Ga. The global heat balance for the Earth then dictates that heat loss was equal to heat production. Given that heat production contributes about half of today's heat loss and that it was twice as large at 2.5 Ga, heat loss was about equal to its present-day value at that time. Using a well-tested model for the thermal evolution of oceanic plates, we relate the rate of melt generation to heat loss and melt thickness at spreading centres (Methods). We show that the rate of melt production cannot have been more than about five times higher than today, far below values required by the ^{129}Xe data. We thus argue in favour of a relatively short burst of mantle activity around the Archaean–Proterozoic boundary, for example, in the 2.6–2.2 Ga time period (Fig. 2d). As shown in the Methods, such intense activity would necessarily be associated with a large heat loss and would induce a dip in ambient mantle temperature if it were long-lived. The mantle ambient temperature data do not support this, and hence provide further support for a short phase of anomalous melt generation.

The large temperatures that prevailed in the late Archaean imply that large melt fractions occurred in mantle upwellings, probably affecting the global rheological behaviour of the mantle. It has been proposed that the mantle may have experienced brief 'mush ocean' episodes[21] that punctuated longer periods of sluggish plate tectonics[22]. The increased overturn rate of cooled material during 'mush oceans' would have resulted in enhanced degassing. It would also have led to larger rates of heat loss and hence rapid cooling. Thus, this anomalous convection regime was self-defeating and could not have been maintained for long. The progressive cooling of the mantle from 2.5 Ga onwards then enabled a stable plate tectonic regime[22,23] and steady-state mantle degassing (Fig. 3).

Several independent geological observations support the operation of a peculiar mantle convection regime in the late Archaean and early Proterozoic[24–26]. For example, the Superior craton saw the repeated accretion of large individual volcanic belts and older terrains at its southern margin in at least five independent events, over very short time intervals of about 10 Myr between[26] 2.70 Ga and 2.65 Ga. Following craton assembly, the very voluminous Matachewan dyke swarm testifies to enhanced magmatic activity and large eruption rates at 2.45 Ga, which are not well accounted for by plate tectonics[27]. Furthermore, the fact the ^{129}Xe/^{130}Xe of the atmosphere has not changed since 2.2 Ga, despite continued large-scale magmatism, indicates that (i) the concentration of Xe in the mantle was lowered during intense degassing periods, and/or that (ii) the initiation of subduction-driven transfer of atmospheric Xe to the mantle during the Archaean–Proterozoic diminished the difference in ^{129}Xe/^{130}Xe between the two reservoirs (Methods).

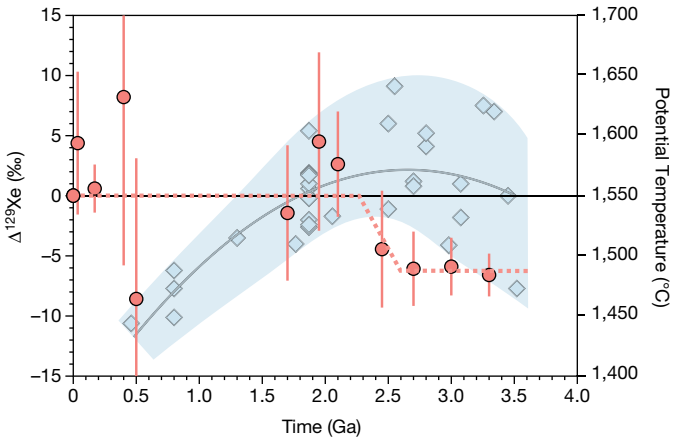

Fig. 3 | Time evolution of the deficit of ^{129}Xe (Δ^{129}Xe) in ancient atmospheric gases compared to petrological estimates of mantle potential temperature (T_P) for non-arc lavas. The data for T_P (light blue diamonds) are taken from ref. [18]. The light grey curve represents the fit through the T_P data, and the light blue shaded area exemplifies the evolution of T_P through time. The filled red circles are the Δ^{129}Xe values as defined in Fig. 1 (error bars, 1σ) and in the main text, and given in Extended Data Table 1.

The period during which Xe was most efficiently degassed from the mantle to the atmosphere (2.6–2.2 Ga) occurred at a time when the Earth was undergoing fundamental environmental changes, including the Great Oxidation Event[28]. An intense period of mantle degassing at that time may therefore have been essential in promoting the transition towards modern Earth-like conditions, which was required for the development of life[2]. Unlike Xe, other volatile elements (water, carbon and nitrogen species) only behave as incompatible elements during redox conditions akin to those of the modern mantle. The near invariance of redox-sensitive elements like vanadium indicates that the redox state of the mantle and associated basalts has remained nearly constant since the middle Archaean to the present[29]. Thus volcanic H_2O, CO_2, N_2 and SO_2 (the main volcanic gas species at low pressures[30]) would have been released into the Archaean atmosphere at rates comparable to that of $^{129}Xe_{DEF}$. The Archaean volcanic flux of CO_2, which is of the order of 6×10^{12} mol yr^{-1} at present[31], would have been in the range 10^{14}–10^{15} mol yr^{-1}, comparable to the anthropogenic flux of CO_2 (7×10^{14} mol yr^{-1}). Such high volcanic gas fluxes could have had tremendous impact on the Archaean environment, providing enormous quantities of CO_2 and SO_2 and possibly triggering the Δ^{34}S peak at that epoch[27]. Enhanced CO_2 (and associated N_2) fluxes could have played a major part in the thermal budget of the Earth's surface[32], by lowering the partial pressure of atmospheric[2] N_2 and by triggering the production of organic matter that ultimately led to the Great Oxidation Event.

Online content

Any methods, additional references, Nature Research reporting summaries, source data, extended data, supplementary information, acknowledgements, peer review information; details of author contributions and competing interests; and statements of data and code availability are available at https://doi.org/10.1038/s41586-019-1745-7.

1. Labrosse, S. & Jaupart, C. Thermal evolution of the Earth: secular changes and fluctuations of plate characteristics. *Earth Planet. Sci. Lett.* **260**, 465–481 (2007).
2. Stüeken, E. E., Kipp, M. A., Scwieterman, E. W., Johnson, B. & Buick, R. Modeling pN_2 through geological time: implications for planetary climates and atmospheric biosignatures. *Astrobiology* **16**, 949–963 (2016).
3. Marty, B. et al. Xenon isotopes in 67P/Churyumov-Gerasimenko show that comets contributed to Earth's atmosphere. *Science* **356**, 1069–1072 (2017).
4. Bekaert, D. V. et al. Archean kerogen as a new tracer of atmospheric evolution: implications for dating the widespread nature of early life. *Sci. Adv.* **4**, eaar2091 (2018).
5. Avice, G. et al. Evolution of atmospheric xenon and other noble gases inferred from Archean to Paleoproterozoic rocks. *Geochim. Cosmochim. Acta* **232**, 82–100 (2018).
6. Meshik, A. P., Hohenberg, C. M., Pravdivtseva, O. V. & Kapusta, Y. S. Weak decay of Ba-130 and Ba-132: geochemical measurements. *Phys. Rev. C* **64**, 035205 (2001).
7. Ozima, M. & Podosek, F. A. *Noble Gas Geochemistry* (Cambridge Univ. Press, 2002).
8. Avice, G., Marty, B. & Burgess, R. The origin and degassing history of the Earth's atmosphere revealed by Archean xenon. *Nat. Commun.* **8**, 15455 (2017).
9. Pujol, M., Marty, B. & Burgess, R. Chondritic-like xenon trapped in Archean rocks: a possible signature of the ancient atmosphere. *Earth Planet. Sci. Lett.* **308**, 298–306 (2011).
10. Mukhopadhyay, S. Early differentiation and volatile accretion recorded in deep-mantle neon and xenon. *Nature* **486**, 101–104 (2012).
11. Péron, S. & Moreira, M. Onset of volatile recycling into the mantle determined by xenon anomalies. *Geochem. Persp. Lett.* **9**, 21–25 (2018).
12. Marty, B., Zimmermann, L., Pujol, M., Burgess, R. & Philippot, P. Nitrogen isotopic composition and density of the Archean atmosphere. *Science* **342**, 101–104 (2013).
13. Zahnle, K. J., Gacesa, M. & Catling, D. C. Strange messenger: a new history of hydrogen on Earth, as told by xenon. *Geochim. Cosmochim. Acta* **244**, 56–85 (2019).
14. Pujol, M., Marty, B., Burgess, R., Turner, G. & Philippot, P. Argon isotopic composition of Archaean atmosphere probes early Earth geodynamics. *Nature* **498**, 87–90 (2013).
15. Bianchi, D. et al. Low helium flux from the mantle inferred from simulations of oceanic helium isotope data. *Earth Planet. Sci. Lett.* **297**, 379–386 (2010).
16. Allard, P. Global emissions of helium-3 by subaerial volcanism. *Geophys. Res. Lett.* **19**, 1478–1481 (1992).
17. Parai, R. & Mukhopadhyay, S. Xenon isotopic constraints on the history of volatile recycling into the mantle. *Nature* **560**, 223–227 (2018): correction. 563, E28 (2018).
18. Herzberg, C., Condie, K. & Korenaga, J. Thermal history of the Earth and its petrological expression. *Earth Planet. Sci. Lett.* **292**, 79–88 (2010).
19. Heber, V. S., Brooker, R. A., Kelley, S. P. & Wood, B. J. Crystal-melt partitioning of noble gases (helium, neon, argon, krypton, and xenon) for olivine and clinopyroxene. *Geochim. Cosmochim. Acta* **71**, 1041–1061 (2007).
20. Porcelli, D. & Elliott, T. The evolution of He isotopes in the convective mantle and the preservation of high ^{3}He/^{4}He ratios. *Earth Planet. Sci. Lett.* **269**, 175–185 (2008).
21. Sleep, N. H. in *Treatise on Geophysics* **9** (ed. Stevenson, D.) 145–170 (Elsevier, 2007).
22. Korenaga, J. Thermal evolution with a hydrating mantle and the initiation of plate tectonics in the early Earth. *Earth Planet. Sci. Lett.* **116**, 1–20 (2011).
23. Tang, M., Chen, K. & Rudnick, R. L. Archean upper crust transition from mafic to felsic marks the onset of plate tectonics. *Science* **351**, 372–375 (2016).
24. Blake, T. S., Buick, R., Brown, S. J. A. & Barley, M. E. Geochronology of a Late Archaean flood basalt province in the Pilbara Craton, Australia: constraints on basin evolution, volcanic and sedimentary accumulation, and continental drift rates. *Precambr. Res.* **133**, 143–173 (2004).
25. Sleep, N. H. & Windley, B. F. Archean plate tectonics: constraints and inferences. *J. Geol.* **90**, 363–379 (1982).
26. Percival, J. A., Stern, R. A. & Skulski, T. Crustal growth through successive arc magmatism: reconnaissance U–Pb SHRIMP data from the northeastern Superior Province, *Canada. Precambr. Res.* **109**, 203–238 (2001).
27. Ciborowski, T. J. R. & Kerr, A. C. Did mantle plume magmatism help trigger the Great Oxidation Event? *Lithos* **246–247**, 128–133 (2016).
28. Holland, H. D. Volcanic gases, black smokers, and the Great Oxidation Event. *Geochim. Cosmochim. Acta* **66**, 3811–3826 (2002).
29. Canil, D. Vanadium in peridotites, mantle redox and tectonic environments: Archean to present. *Earth Planet. Sci. Lett.* **195**, 75–90 (2002).
30. Gaillard, F., Scaillet, B. & Arndt, N. T. Atmospheric oxygenation caused by a change in volcanic degassing pressure. *Nature* **478**, 229–232 (2011).
31. Marty, B. & Tolstikhin, I. N. CO_2 fluxes from mid-ocean ridges, arcs and plumes. *Chem. Geol.* **145**, 233–248 (1998).
32. Kasting, J. F. Faint young Sun redux. *Nature* **464**, 687–689 (2010).

Methods

Deficit of ^{129}Xe in Archaean air relative to modern air, reservoirs and fluxes

Δ^{129}Xe is the deviation of the sample ^{129}Xe/^{130}Xe ratio from the modern atmospheric ^{129}Xe/^{130}Xe ratio, in ‰ (Fig. 1). Modern atmospheric xenon is mass-dependently fractionated relative to ancient atmosphere[4,5,8,9]. Because atmospheric ^{129}Xe is contributed by a monoisotopic nuclear effect (the decay of ^{129}I), its variation can be identified from mass-dependent isotopic fractionation by comparison to the adjacent stable Xe isotopes. Following Pujol et al.[9], the isotope ratios are normalized to the modern Xe isotope composition, and the slopes of the fractionation trends (as well as the original data) are listed in refs. [4,5,8,9] (original Xe data are reported in https://zenodo.org/record/3378722#.Xa6cay3pNvF).

Δ^{129}Xe is the distance between the measured δ^{129}Xe value (green dot, Fig. 1) and the equivalent value sitting on the fractionation line at mass 129 (white dot, Fig. 1). Values of Δ^{129}Xe different from 0 are identified for three samples having ages around 3 Ga (Extended Data Table 1). Other samples have Δ^{129}Xe values that are not statistically different from the modern atmosphere composition. Most of these samples were analysed only once and as such the resulting errors are comparatively large. For the three samples above, we computed a mean error-weighted Δ^{129}Xe value of (−6.3 ± 2.5)‰ (95% CI) for the period 3.3–2.7 Ga.

The amount of ^{129}Xe that was missing in the Archaean atmosphere, denoted $^{129}Xe_{DEF}$, is computed from the mean Archaean Δ^{129}Xe value, the modern Xe inventory of the atmosphere, and the isotopic composition of modern atmospheric Xe (Extended Data Table 2). Taking the Archaean atmospheric ratio of 6.455 (obtained by subtracting 6.3‰ from the modern ^{129}Xe/^{130}Xe ratio, after correction for mass-dependent isotopic fractionation) instead of the modern value[7] of 6.496 would make a negligible difference compared to uncertainties in Δ^{129}Xe values. We also considered a non-conservative atmosphere from which 2.5 times the modern Xe inventory is lost to space, as suggested by the temporal evolution of Xe MDF (Extended Data Fig. 1). ^{129}Xe degassed from the mantle that changes the atmospheric Xe isotopic composition is labelled $^{129}Xe_{XS}$. The average yearly flux of $^{129}Xe_{XS}$ was simply computed by dividing $^{129}Xe_{DEF}$ by 3×10^9 yr (Extended Data Table 2).

The modern mantle flux of $^{129}Xe_{XS}$, $\varphi^{129}Xe_{XS}$, is computed as:

$$\varphi^{129}Xe_{XS} = \varphi^{3}He_{mantle} \times (^{130}Xe/^{3}He)_{mantle} \times [(^{129}Xe/^{130}Xe)_{mantle} - (^{129}Xe/^{130}Xe)_{atm}] \quad (1)$$

with $(^{129}Xe/^{130}Xe)_{atm} = 6.496$ (ref. [7]). The fluxes were computed for two different mantle sources, namely mid-ocean ridge basalt (MORB; ^{129}Xe/^{130}Xe = 7.8, ref. [11]), and mantle plume (^{129}Xe/^{130}Xe = 7.0, ref. [10]). The resulting global value, 0.89 ± 0.47 mol yr^{-1}, encompasses both estimates within uncertainties (Extended Data Table 2). Note that this value is an upper limit since it assumes a end-member ratio for mantle ^{129}Xe/^{130}Xe.

Cometary contribution

We test here the possibility that the $^{129}Xe_{DEF}$ was compensated by the delivery of cometary Xe. The analysis of volatiles released by comet 67P/Churyumov–Gerasimenko (67P/C–G) suggests[3] that comets are rich in xenon and particularly in ^{129}Xe. A large amount of ^{129}Xe could have been delivered by cometary impacts in the time interval 3.0–2.0 Ga. Assuming that the xenon data from 67P/C–G[3,33] (^{129}Xe/^{130}Xe = 7–8, Xe/$H_2O = 2.4 \times 10^{-7}$, H_2O concentration ~20 wt%, density 0.55 g cm^{-3}) are representative of the cometary reservoir, a single comet with a diameter of ~260 km impacting the Earth could have delivered the amount of ^{129}Xe missing in the Archaean atmosphere. For comparison, the impactor that made the 2.02-Ga-old Vredefort impact structure (the second largest one preserved on Earth) might have been much smaller, around 10–20 km in diameter[34]. Several cometary impacts would have resulted in a similar effect, without leaving scars on Earth if they occurred in the oceans, or if comets exploded in the upper atmosphere. However, this possibility is not consistent with the progressive isotope evolution of palaeo-atmospheric xenon, which is best accounted for by escape to space[5,8,9], whereas addition of cometary Xe would have forced Archaean atmospheric Xe towards a primitive composition rather than a modern atmospheric one. We therefore consider the addition of cometary ^{129}Xe during the Archaean to be insignificant compared to the contribution from mantle degassing.

Mantle degassing state

We evaluate here how much mantle Xe should have been lost from the 3-Ga mantle through time in order to supply missing ^{129}Xe to the atmosphere since 3 Ga ($^{129}Xe_{DEF} = 2.6 \times 10^{10}$ mol for a closed system atmosphere, and 9×10^{10} mol in the case of atmospheric escape, Extended Data Table 2). We consider two mantle sources[10,11], MORB-like (^{129}Xe/^{130}Xe = 7.8) and mantle-plume-like (^{129}Xe/^{130}Xe = 7.0). The mantle Xe contents are scaled to those of ^{3}He. The MORB source ^{3}He content is computed from the ^{3}He flux to the oceans and subaerial volcanoes[15,16], the magma generation rate at ridges (21 km^3 yr^{-1}) and an average partial melting rate of 12% (ref. [35]). The plume source content is derived from the difference in the helium isotope ratios and in the U, Th contents between MORB and plume sources (ref. [35], see ref. [36] for comparable values). Two cases are considered, the modern mantle and the ancient, pre-subduction mantle. For the latter, we use ^{129}Xe/^{130}Xe = 14 (±1) which is our estimate for pre-atmospheric contamination of mantle xenon (based on Xe isotope correlations for CO_2 well gases; compare ref. [37]; Extended Data Fig. 2), and we correct the ^{130}Xe/^{3}He ratio for 80% atmospheric contribution, assumed to have taken place quantitatively in the last billion years (see Methods section 'Numerical modelling' below). We finally compute the lost fraction for each reservoir and for each scenario (Extended Data Table 3). In all scenarios, a MORB-type reservoir would have lost between 59% and 99.4% mantle Xe. A plume source reservoir would have lost between 3.5% and 64% Xe. A pure depleted MORB-type composition at 3 Ga is unlikely given the timing of continental crust growth (which was the primary cause of mantle depletion), and a modern-like Xe isotope composition might not have prevailed before 1 Ga. Hence it may be relevant to consider a pure ocean island basalt (OIB)-like, or mixed MORB-plume composition, with atmospheric Xe recycling taking place in the last billion years, yielding a moderate 3-Ga mantle degassing state of ~50% or less. Thus the Archaean mantle could have been richer by a factor of approximately ≤2 in xenon compared to the modern mantle.

Higher concentrations of Xe in the Archaean mantle relative to its present-day budget could potentially lower the amount of mantle degassing necessary to account for the evolution of the ^{129}Xe deficit in the Archaean atmosphere. We have estimated above that the concentration of xenon could have been ≤50% higher at 3 Ga based on mass balance of the mantle reservoir. However, models investigating the time evolution of the ^{3}He/^{4}He of the mantle, for example, require mantle ^{3}He concentrations to be higher during the Archaean[20,37]. Therefore, we have attempted to define independently the maximum amount of Xe that could be present within the Archaean mantle by constraining it with Ne isotopes.

Neon provides a useful tool for constraining the concentration of Xe in different reservoirs as is not efficiently recycled to the mantle (in contrast to Ar, Kr and Xe; ref. [38]) and has been retained in the atmosphere throughout Earth's history (in contrast to He). An additional problem with scaling our calculations against He would be that, unlike the case of Ne, the isotopic composition of the mantle end-member is not known. For Ne, if the mantle was enriched in the Archaean (3.3 Ga) relative to the modern day by a factor of 10–20, as has been suggested for ^{3}He, then the progressive degassing of mantle Ne to the atmosphere with time will result in a change in the isotopic ratio of the atmosphere, as there is a discernible difference in the Ne isotopes between the solar/chondritic ^{20}Ne/^{22}Ne ratio of the mantle (12.7–13.4, refs. [39–41]) and the atmosphere (9.80). However, as of yet, no Archaean aged samples have

shown deviations in Ne isotopes from the modern atmosphere[5], indicating limited contribution of the mantle Ne signature to the atmosphere since 3.3 Ga.

We define the maximum possible Ne enrichment factor for the Archaean mantle that could still preserve the modern day atmospheric composition through time by using concentration weighted isotopic mixing calculations. First, we assume that any enrichment in Ne concentrations within the Archaean mantle relative to the present will be ultimately degassed and retained in the atmosphere. Thus, if the mantle was 10 times more enriched in Ne during the Archaean, the Archaean atmosphere must be depleted by the same amount. We take the minimum measured $^{20}Ne/^{22}Ne$ ratio measured within 3.3-Ga quartz-hosted fluid inclusions to be that of the Archaean atmosphere (9.64 ± 0.05; ref. [5]). The mantle $^{20}Ne/^{22}Ne$ is defined as either having a solar (13.4; ref. [41]) or a chondritic-like (12.7; ref. [40]) composition. We determine that to raise the $^{20}Ne/^{22}Ne$ of the Archaean atmosphere from 9.59 to the modern value of 9.8 would require 1.60×10^{14} mol of mantle ^{20}Ne to be degassed to the atmosphere assuming the mantle has solar $^{20}Ne/^{22}Ne$, and 1.96×10^{14} mol if the mantle has chondritic $^{20}Ne/^{22}Ne$. The amount of mantle neon degassed to the atmosphere since 3.3 Ga can be expressed as:

$$^{20}Ne_{degassed} = {}^{20}Ne_{MA} - {}^{20}Ne_{AA} = {}^{20}Ne_{AI}\left\{\frac{[(^{20}Ne/^{22}Ne)_{AA} - (^{20}Ne/^{22}Ne)_{MA}]}{[(^{20}Ne/^{22}Ne)_{AA} - (^{20}Ne/^{22}Ne)_{mantle}]}\right\} \quad (2)$$

where subscripts AA, MA, AI and mantle refer to Archaean atmosphere, modern atmosphere, atmospheric inventory and mantle, respectively. Readmitting the amount of degassed Ne back to the mantle would result in the mantle during the Archaean being enriched by a factor of 1.2–3.8 times the present concentrations (mantle inventories obtained from end-member mantle ^{20}Ne concentrations[36,42], and a mantle mass of 4×10^{27} g) assuming a solar mantle, and 1.2–4.4 if the mantle Ne is chondritic. The large range in these estimates is controlled primarily by the large uncertainty on the concentration of Ne in the present-day mantle[36,42].

Potential impact of Archaean degassing on atmospheric noble gases

We tested the effect of intensive mantle degassing during the Archaean on the evolution of the atmospheric $^{40}Ar/^{36}Ar$ ratio. We carried out a mass balance calculation based on the mantle noble-gas composition on one hand, and on the other, the amount of $^{129}Xe_{DEF}$ in the atmosphere. We considered two mantle sources, MORB-like and plume-like, with noble-gas end-member compositions[10,11]. The respective $^{40}Ar/^{36}Ar$ ratios were computed at 3 Ga (correcting for radiogenic ^{40}Ar produced afterwards), and we considered a pre-subduction, Archaean $^{129}Xe/^{130}Xe$ ratio of 14 (Extended Data Fig. 2). Results suggest that the contribution of Archaean mantle degassing to the ^{40}Ar atmospheric inventory was of the order of a few per cent (Extended Data Table 3). We tested the effect of 5% and 10% ^{40}Ar inventory degassing during a sudden release of ^{129}Xe at 2.6–2.2 Ga, with a K-Ar box model similar to that used by Pujol et al.[14] that includes early degassing and crustal growth. The evolution curves are depicted in Extended Data Fig. 3. In principle, a jump of the Ar isotopic ratio around that period of time could be observable, but uncertainties related to the contribution of ^{40}Ar produced in situ in samples could mask such an effect. Thus we conclude that a massive Archaean mantle degassing event would not have drastically affected the radiogenic ^{40}Ar budget of the atmosphere.

During Archaean degassing, fissiogenic Xe isotopes were also released together with $^{129}Xe_{XS}$ from the mantle to the atmosphere. In mantle-derived samples, $^{129}Xe/^{130}Xe$ correlates with $^{136}Xe/^{130}Xe$ with a slope of 3.0 for both MORB and plume sources[10,11], as a result of contributions of radiogenic ^{129}Xe and fissiogenic ^{136}Xe ($^{136}Xe_f$). An Archaean $\Delta^{129}Xe$ value of −6‰ (Extended Data Table 1) would therefore correspond to a deficit of $^{136}Xe_f$ of about −2‰ in Archaean air. Such a variation would be barely detectable in ancient samples. Archaean samples analysed so far[4,5,8] present positive $\Delta^{136}Xe_f$ values of +30‰ (Barberton sample[5]) and higher[8], with fission spectra consistent with production from ^{238}U fission[5]. Thus any potential effect of mantle degassing is likely to be masked by the inheritance of fissiogenic Xe from the trapped crustal fluids and/or the in situ production from ^{238}U fission after emplacement of the rocks at the surface. This problem would prevent detection of any effect on the Archaean atmospheric composition of fissiogenic Xe.

Numerical modelling

We consider three scenarios around the evolution curve of the isotopic composition of atmospheric Xe (Extended Data Fig. 1), which has been modelled to follow a power law defined by $y = 0.238x^{3.41}$ (ref. [4]). New data on the isotopic composition of ancient atmosphere Xe from fluid inclusions in hydrothermal quartz have been recently published[5] that support the validity of this evolution curve. Also reported in Extended Data Fig. 1 is the theoretical amount of extra ATM_{Xe} in the atmosphere scaled on Xe isotopic evolution, where ATM_{Xe} stands for the total inventory of Xe in the present-day atmosphere. Over the lifetime of the atmosphere, ~10 ATM_{Xe} would have been lost to space.

In the first scenario, we consider that Xe degassing from the mantle occurred after Xe loss to space ended. This implies that the $\Delta^{129}Xe$ remained constant (at (−6.3 ± 2.5)‰) from 3 Ga to 1 Ga, before $\Delta^{129}Xe$ was raised to 0‰ solely through mantle degassing. In this case, mantle degassing takes place while the Xe isotope signature of the atmosphere is already modern-like, with no concomitant loss to space.

In the second scenario, we consider that Xe degassing from the mantle (with $\Delta^{129}Xe$ varying from (−6.3 ± 2.5)‰ to 0‰) occurred at 3 Ga, when the atmosphere was mass dependently fractionated by −10‰ u^{-1} and had about 3.5 times the present-day inventory of atmospheric Xe (Extended Data Fig. 1, right hand *y* axis). In this case, given that Xe is more abundant in the atmosphere than in the first scenario, the total amount of mantle-derived ^{129}Xe required to fill the ^{129}Xe deficit ($^{129}Xe_{DEF}$) is also larger than in the first scenario.

The first and second scenarios do not represent real world conditions, as they assume that degassing and loss did not occur simultaneously, but they are useful in setting the boundary conditions to this model. In the third scenario, we produce an iterative model combining progressive loss and MDF of atmospheric Xe (Extended Data Fig. 1) with the evolution of $\Delta^{129}Xe$ (Fig. 2). To model the latter, we test three possibilities by fitting $\Delta^{129}Xe$ data with either power law, exponential, power-law or ramp functions (Fig. 2A–D). At each step of the iteration (*i*), the atmosphere is allowed to evolve by both loss to space and MDF (Extended Data Fig. 4). The $^{129}Xe/^{130}Xe$ ratio is then computed by using both $\Delta^{129}Xe$ (*i* − 1) and $\Delta^{129}Xe$ (*i*). The contribution of mantle-derived ^{129}Xe ($^{129}Xe_{XS}$) to the atmospheric budget of ^{129}Xe from step *i* − 1 to step *i* is then calculated given the equation:

$$M_{contrib^{129}Xe} = \frac{(^{129}Xe/^{130}Xe)_i - (^{129}Xe/^{130}Xe)_{i-1}}{(^{129}Xe/^{130}Xe)_M - (^{129}Xe/^{130}Xe)_{i-1}} \quad (3)$$

where $(^{129}Xe/^{130}Xe)_i$ and $(^{129}Xe/^{130}Xe)_{i-1}$ are the $^{129}Xe/^{130}Xe$ of the atmosphere at steps *i* and *i* − 1, respectively, and $(^{129}Xe/^{130}Xe)_M$ is the $^{129}Xe/^{130}Xe$ of the mantle source. The amount (in mol) of mantle-derived ^{129}Xe degassed into the atmosphere between step *i* − 1 and step *i* is then calculated as:

$$M_{^{129}Xe} = M_{contrib^{129}Xe} \times ATM_{^{129}Xe_i} \quad (4)$$

where $ATM_{^{129}Xe_i}$ is the total amount (in mol) of ^{129}Xe in the atmosphere at step *i* given the evolution curve of Xe loss and $^{129}Xe/^{130}Xe$ computed

from the evolution curve of atmospheric Xe isotopes and $\delta^{129}Xe_{def(i)}$. However, determining the ($^{129}Xe/^{130}Xe$) of the mantle is not straightforward, given that this ratio also evolved through time by ^{129}Xe production through radioactive decay of now extinct ^{129}I and recycling of atmospheric Xe into the solid Earth. Given that the half-life of ^{129}I is short ($T_{1/2}$ = 15.7 Myr), the whole budget of $^{129}Xe^*$ (that is, ^{129}Xe produced by the decay of ^{129}I) should have been established early in Earth's history, within the first ~100 Myr. The recycling of atmospheric Xe to the mantle is considered to be extensive, with the present-day inventory of Xe in the mantle dominated by 80%–90% recycled modern atmosphere[10,11]. Correcting the mantle $^{129}Xe/^{130}Xe$ (7.8) for the contribution of recycled atmosphere (80%–90%) would yield a $^{129}Xe/^{130}Xe$ in the range of 13–17 for the primitive convective mantle. The initial $^{129}Xe/^{130}Xe$ of the convective mantle can also be estimated from $^{128}Xe/^{130}Xe$ versus $^{129}Xe/^{130}Xe$ correlations in magmatic CO_2 well gases (ref. [43], Extended Data Fig. 2). The $^{128}Xe/^{130}Xe$ of the initial mantle is taken as the chondritic value ($^{128}Xe/^{130}Xe_{AVCC}$ = 0.5073 ± 0.0038, where suffix AVCC refers to Average Carbonaceous Chondrite, ref. [7]). Extrapolating the $^{129}Xe/^{130}Xe$ to $^{128}Xe/^{130}Xe_{AVCC}$ yields a $^{129}Xe/^{130}Xe_{initial}$ between 13 and 15, in good agreement with independent estimates from the fraction of recycled atmosphere in the mantle. Note that these estimates assume that the atmospheric Xe component in the mantle has a modern atmospheric composition. If Xe was extensively recycled to the mantle while the Xe composition of the atmosphere was still evolving, then estimating the $^{129}Xe/^{130}Xe$ of the mantle during the Archaean becomes more complicated. However, Parai and Mujhopadhyay[17] proposed that substantial full-scale recycling of atmospheric xenon into the solid Earth could not have occurred before 2.5 Ga, given that (i) the isotopic composition of atmospheric Xe progressively evolved through time by MDF and reached the modern composition around 2 Ga (Extended Data Fig. 1), and (ii) the Xe atmospheric component in the present-day mantle is indistinguishable from modern atmosphere. Although the recycling history of atmospheric Xe into the mantle between 2.5 Ga and 1 Ga is not known, constraints on the amount of Xe being transported into the solid Earth over time through atmospheric recycling have been recently set via numerical modelling of Xe evolution in the mantle–atmosphere system (Extended Data Fig. 5, ref. [17]). While some small scale recycling of atmospheric Xe to the mantle might have occurred before 2.5 Ga, it would have had a limited effect on the budget and isotopic composition of mantle Xe, and we therefore consider our estimates of mantle $^{129}Xe/^{130}Xe$ between 13 and 15 during the Archaean to be valid.

The $\Delta^{129}Xe$ evolution curves are represented in Fig. 2. We also provide the time evolution of the atmospheric $^{129}Xe/^{130}Xe$ ratio and the flux φ of mantle-derived ^{129}Xe ($\varphi^{129}Xe$) to the atmosphere. The $^{129}Xe/^{130}Xe$ ratio might not vary monotonically because two independent processes (namely MDF of the atmosphere and mantle degassing) are causing this ratio to vary (decrease and increase through time, respectively). In the case of a short burst, the $^{129}Xe/^{130}Xe$ ratio would first decrease due to MDF, and increase during the burst (during which MDF is still ongoing but mantle degassing dominates), and then decrease again because of MDF. However, the $\Delta^{129}Xe$ would either remain stable during periods of limited mantle degassing, or increase towards 0 during period(s) of intense mantle degassing. The results of the different model versions are summarized in Extended Data Table 4.

Rate of melt production by mantle convection

For a physical model of the Earth's secular thermal evolution, one needs an equation that relates heat loss to temperature. Many past efforts have been based on physical models of sea floor spreading that have been calibrated using present-day plate characteristics[1,44]. These models must be tuned to account for changes of plate structure, density and rigidity arising from the larger temperatures and amounts of melting that prevailed in the past. A major difficulty is that plate velocities and sizes vary by about one order of magnitude on modern Earth[1,22], so that extrapolating plate tectonics far back in time is uncertain. Other models of secular cooling have relied on first-principles convection calculations, but it has proven difficult to reproduce plate tectonics owing to the large lithospheric strength that must be overcome to initiate subduction. Thus, quantitative models for mantle convection in the Archaean must be regarded as tentative[22,44,45].

Here, we circumvent this difficulty by deriving a general relationship between heat flux and melt production rate. We assume that the degassing of basaltic melts proceeds to completion so that the degassing rate is proportional to the melt generation rate, which leads to a lower bound on the melting rate. A general equation for the surface heat flux can be written for all convection regimes save the 'stagnant lid' one. In the latter regime, convection develops below a rigid layer that caps the whole planet and does not allow surface motions. For all other regimes, the basic principle is that cooling is effected in a thermal boundary layer at the top of the mantle, where vertical velocities are negligible. Heat loss is therefore due to conduction and depends on the residence time of material at the surface. This principle has been thoroughly tested in laboratory experiments and numerical calculations, as well as on the current oceanic plates[45]. Denoting the mantle potential temperature by T_P, surface temperature by T_S, the total heat loss due to convection is:

$$Q_0 = \psi(f) S_o k \frac{T_P - T_S}{\sqrt{\pi \kappa \tau_M}} \quad (5)$$

where k is thermal conductivity, κ is thermal diffusivity and S_o is the total surface of oceanic plates involved in convective motions. A key parameter is τ_M, which is the maximum age of sea floor at the Earth's surface. $\psi(f)$ depends on the distribution of sea floor ages, which is described by some function f:

$$f(t/\tau_M) = \mathrm{d}S/\mathrm{d}t \quad (6)$$

which is the surface increment between ages t and $t + \mathrm{d}t$. The current age distribution on Earth is 'triangular', such that it decreases linearly from a maximum at $t = 0$ to zero at $t = \tau_M$. This contrasts with standard convective systems for which the age distribution is 'rectangular'[40], that is, constant between $t = 0$ and $t = \tau_M$. The difference between the two distributions has a small impact on factor $\psi(f)$ in equation (4), which is not important for this discussion. The rate of sea floor generation, denoted C_A, is such that:

$$S_o = C_A \tau_M \int_0^1 f(u)\mathrm{d}u \quad (7)$$

The age distribution has again a minor impact on the result (a maximum factor of two). The thickness of melt produced, denoted H, may be calculated from thermodynamics[45] as a function of the mantle potential temperature T_P for a given mantle composition. The volume of melt produced per unit time in a plate tectonic regime is equal to:

$$\varphi = C_A H \quad (8)$$

This leads to a relationship between the melt production rate and heat loss:

$$\varphi = \lambda \frac{Q_o H}{(T_P - T_S)\sqrt{\kappa \tau_M}} \quad (9)$$

where λ is a constant.

We may now evaluate the conditions that are needed for a ≥10-fold change in melting rate. As shown in the main text, the Archaean heat flux was about equal to today's value. The mantle temperature was about 200 °C higher than today but this only implies an ~20% change of the overall temperature contrast ($T_P - T_S$), which does not change the present argument. According to ref. [21], the thickness of melt produced in hot Archaean mantle was in the range 25–35 km, corresponding to at least a threefold increase with respect to the present-day value. In order to achieve a ≥10-fold increase in melt production rate, the maximum age of oceanic plates would need to be decreased by a factor of at least $3^2 = 9$. Today, this maximum age is 180 Myr and it is not clear how plate tectonics could have operated over less than 20 Myr in the Archaean.

We have focused on the heat flow through oceanic plates and have not discussed the potential influence of continents. This is not needed here for the following reason. Continental heat flow is very close to the amount of heat released by radioactive decay in crustal rocks[45], so that our conclusion that the Archaean oceanic heat flow had to be about equal to mantle heat production still stands.

A short-lived burst of mantle activity

Enhanced degassing necessarily implies enhanced melting and heat loss, and hence enhanced cooling of the mantle, which must lead to a dip of mantle temperature if it is maintained for a long time. The thermal impact of a pulse of high mantle activity may be difficult to detect, however. Mantle temperatures have been determined with a precision of about ±60 °C (ref. [46]) at time steps of a few hundred million years and exhibit scatter (about 100–150 °C) for ages older than 2.0 Ga (ref. [21]). With the current net energy loss of Earth (equal to heat loss minus heat production), it takes about one billion years for the mantle temperature to drop by 100 °C. A net energy loss that is ten times larger would lead to the same temperature drop in 100 Myr, at the detection limit of the current temperature data. Combining heat balance arguments with constraints from ambient mantle temperatures and ^{129}Xe data should allow tight bounds to be set on the intensity and duration of anomalous mantle activity (Fig. 3).

Data availability

The sample description and Xe data are available at https://zenodo.org/record/3378722#.Xa6cMi3pNvE.

Code availability

The Matlab code for modelling the degassing rate of Xe from the mantle is available at https://zenodo.org/record/3381874#.Xa6cey3pNvE.

33. Rubin, M. et al. Krypton isotopes and noble gas abundances in the coma of comet 67P/Churyumov-Gerasimenko. *Sci. Adv.* **4**, eaar6297 (2018).
34. Reimold, W. U. & Gibson, R. L. Geology and evolution of the Vredefort impact structure, South Africa. *J. Afr. Earth Sci.* **23**, 125–162 (1996).
35. Tolstikhin, I. N. & Marty, B. The evolution of terrestrial volatiles: a view from helium, neon, argon and nitrogen isotope modelling. *Chem. Geol.* **147**, 27–52 (1998).
36. Halliday, A. N. The origins of volatiles in the terrestrial planets. *Geochim. Cosmochim. Acta* **105**, 146–171 (2013).
37. Gonnermann, H. M. & Mukhopadhyay, S. Preserving noble gases in a convective mantle. *Nature* **459**, 560–563 (2009).
38. Holland, G. & Ballentine, C. J. Seawater subduction controls the heavy noble gas composition of the mantle. *Nature* **441**, 186–191 (2006).
39. Ballentine, C. J., Marty, B., Sherwood Lollar, B. & Cassidy, M. Neon isotopes constrain convection and volatile origin in the Earth's mantle. *Nature* **433**, 33–38 (2005).
40. Moreira, M. & Charnoz, S. The origin of the neon isotopes in chondrites and on the Earth. *Earth Planet. Sci. Lett.* **433**, 249–256 (2016).
41. Williams, C. D. & Mukhopadhyay, S. Capture of nebular gases during Earth's accretion is preserved in deep-mantle neon. *Nature* **565**, 78–81 (2019).
42. Marty, B. The origins and concentrations of water, carbon, nitrogen and noble gases on Earth. *Earth Planet. Sci. Lett.* **313–314**, 56–66 (2012).
43. Caffee, M. W. et al. Primordial noble gases from Earth's mantle: identification of a primitive volatile component. *Science* **285**, 2115–2118 (1999).
44. Korenaga, J. in *Archean Geodynamics and Environments* (eds Benn, K., Mareschal, J. C. & Condie, K. C.) 7–32 (Geophys. Monogr. Ser. **164**, AGU, 2006).
45. Jaupart, C. & Mareschal, J.-C. in *Treatise on Geophysics* **6** (ed. Stevenson, D.) 217–251 (Elsevier, 2007).
46. Herzberg, C. & Asimow, P. D. PRIMELT3 MEGA.XLSM software for primary magma calculation: peridotite primary magma MgO contents from the liquidus to the solidus. *Geochem. Geophys. Geosyst.* **16**, 563–578 (2015).

Acknowledgements This study was supported by the European Research Council (Photonis Advanced Grant no. 695618). We thank G. Avice for discussions, and the Fondation des Treilles for providing a congenial environment in which to discuss these concepts with colleagues.

Author contributions B.M. developed the ideas presented in the manuscript. D.B. wrote the Matlab script for the numerical modelling, M.B. contributed the geological context and developed noble-gas constraints on atmospheric evolution. C.J. developed the thermal model. All authors participated in the writing of the manuscript.

Competing interests The authors declare no competing interests.

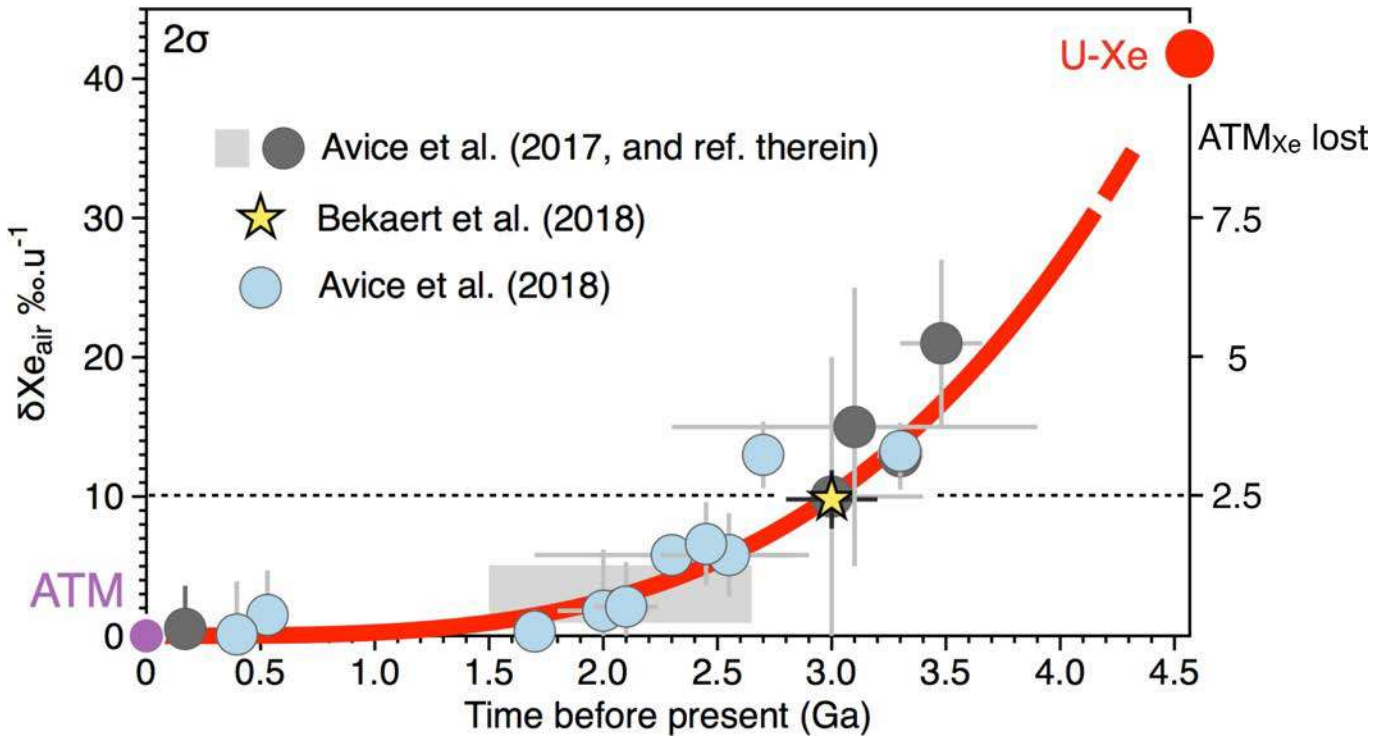

Extended Data Fig. 1 | MDF of atmospheric Xe with time relative to the modern atmosphere. Grey and blue data points[5,8] define the evolution (red curve) of atmospheric Xe mass-dependent fractionation (MDF)[4]. The left-hand *y* axis shows the isotopic fractionation of atmospheric Xe (δXe_{air}) in units of ‰ per atomic mass unit (u). The right-hand *y* axis represents multiples of the Xe inventory of the modern atmosphere, ATM_{Xe}. Error bars, ±2σ. The purple point on the left-hand side (ATM) is the modern atmospheric composition, the red dot on the right-hand side (U-Xe) is the primordial composition of atmospheric xenon[3], the grey-shaded area shows the data range from ref. [5] and references therein, and the dotted horizontal line gives the MDF value; the ATM_{Xe} values correspond to a mean age of 3 Ga.

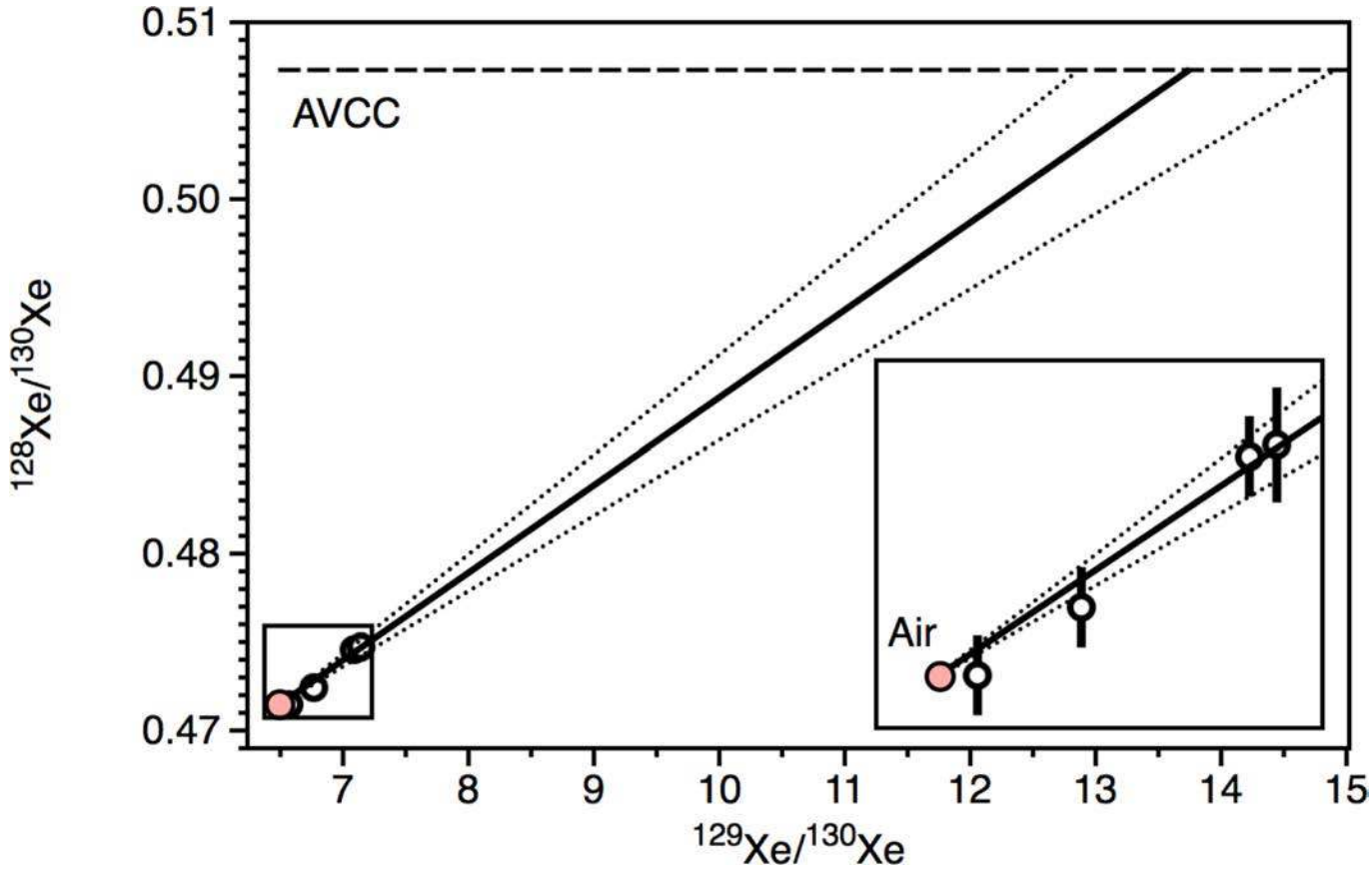

Extended Data Fig. 2 | Plot of $^{128}Xe/^{130}Xe$ versus $^{129}Xe/^{130}Xe$ for CO_2 well gases. Open circle data points are from ref. [38], and the pink filled circle shows the isotopic composition of air (error bars, 1σ). The boxed area at lower left is shown magnified in the inset. There is a correlation between the excess ^{129}Xe and ^{128}Xe (thick line, dotted thin lines define the error envelope, 95% CI) that can be used to extrapolate the primordial $^{129}Xe/^{130}Xe$ of the mantle source for an AVCC-like $^{128}Xe/^{130}Xe$ (dashed black line).

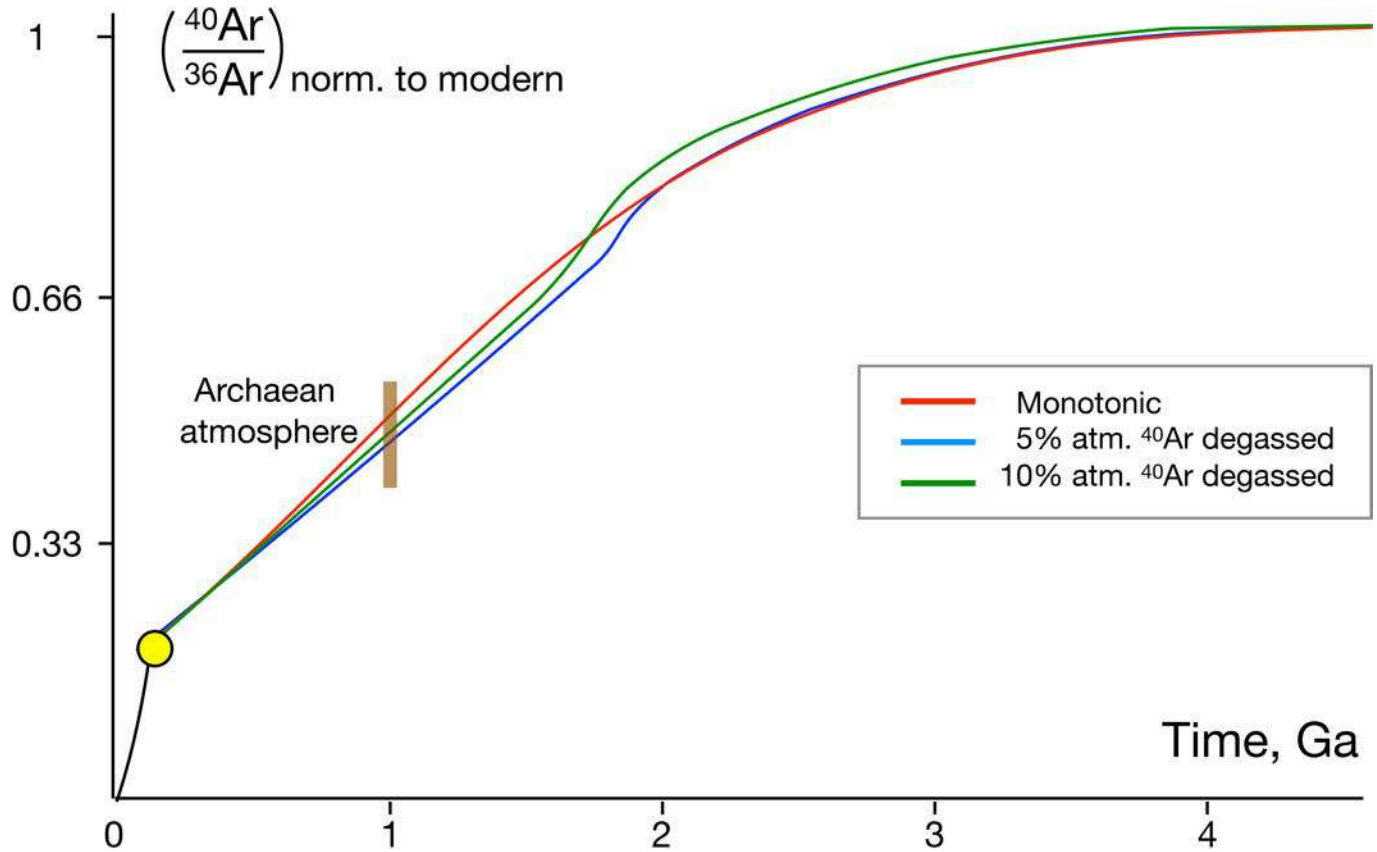

Extended Data Fig. 3 | Modelled evolution of the atmospheric $^{40}Ar/^{36}Ar$ ratio as a function of time following a mantle degassing event between 2.6 Ga and 2.2 Ga. The values are scaled to $^{129}Xe_{DEF}$, and are shown with different contributions of mantle ^{40}Ar: 0% ('Monotonic'), 5% and 10%. Atmospheric $^{40}Ar/^{36}Ar$ ratios are normalized to the present-day value of 298.6, and the evolution curves were adjusted in order to yield the modern value. The Archaean atmosphere's value is from ref. [14]. The yellow dot marks the end of catastrophic degassing and the start of continuous degassing, following ref. [14].

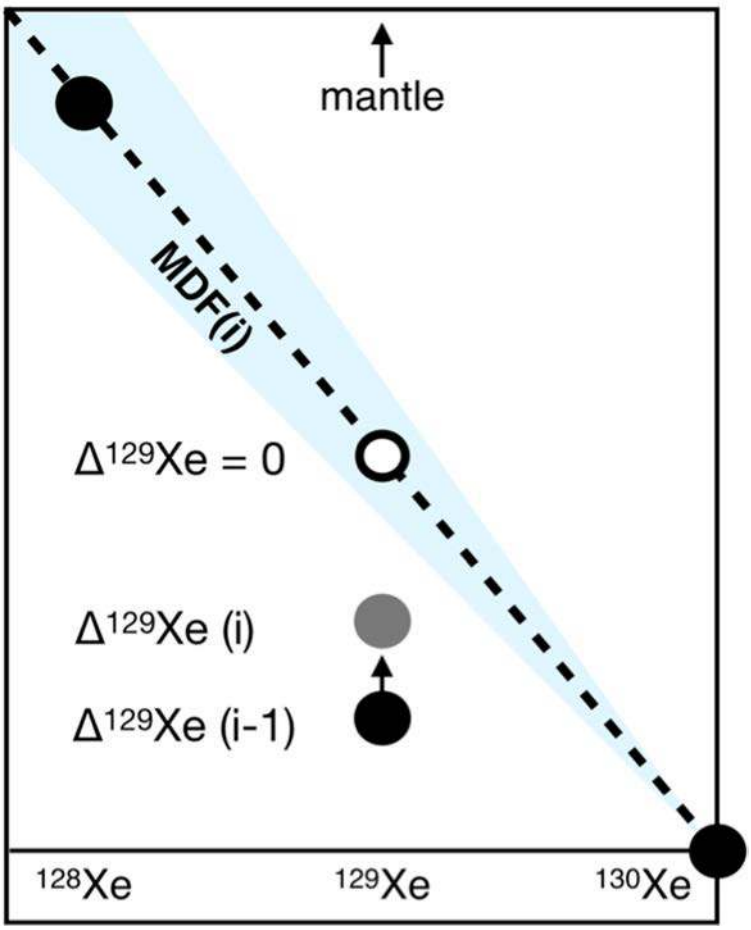

Extended Data Fig. 4 | Schematic representation of the method used to calculate the contribution of mantle-derived ^{129}Xe to the atmospheric budget of ^{129}Xe from step *i* − 1 to step *i*. The format is the same as in Fig. 1, where the *y* axis corresponds to δXe_{air} (only indicative here).The 'mantle' arrow indicates that the $^{129}Xe/^{130}Xe$ of the mantle end-member is high, and would plot off-graph in this space. $\Delta^{129}Xe$ values at each step of the simulation are reported on the left of the corresponding data points. The dashed line corresponds to the MDF line, with the shaded blue area representing the corresponding error envelope.

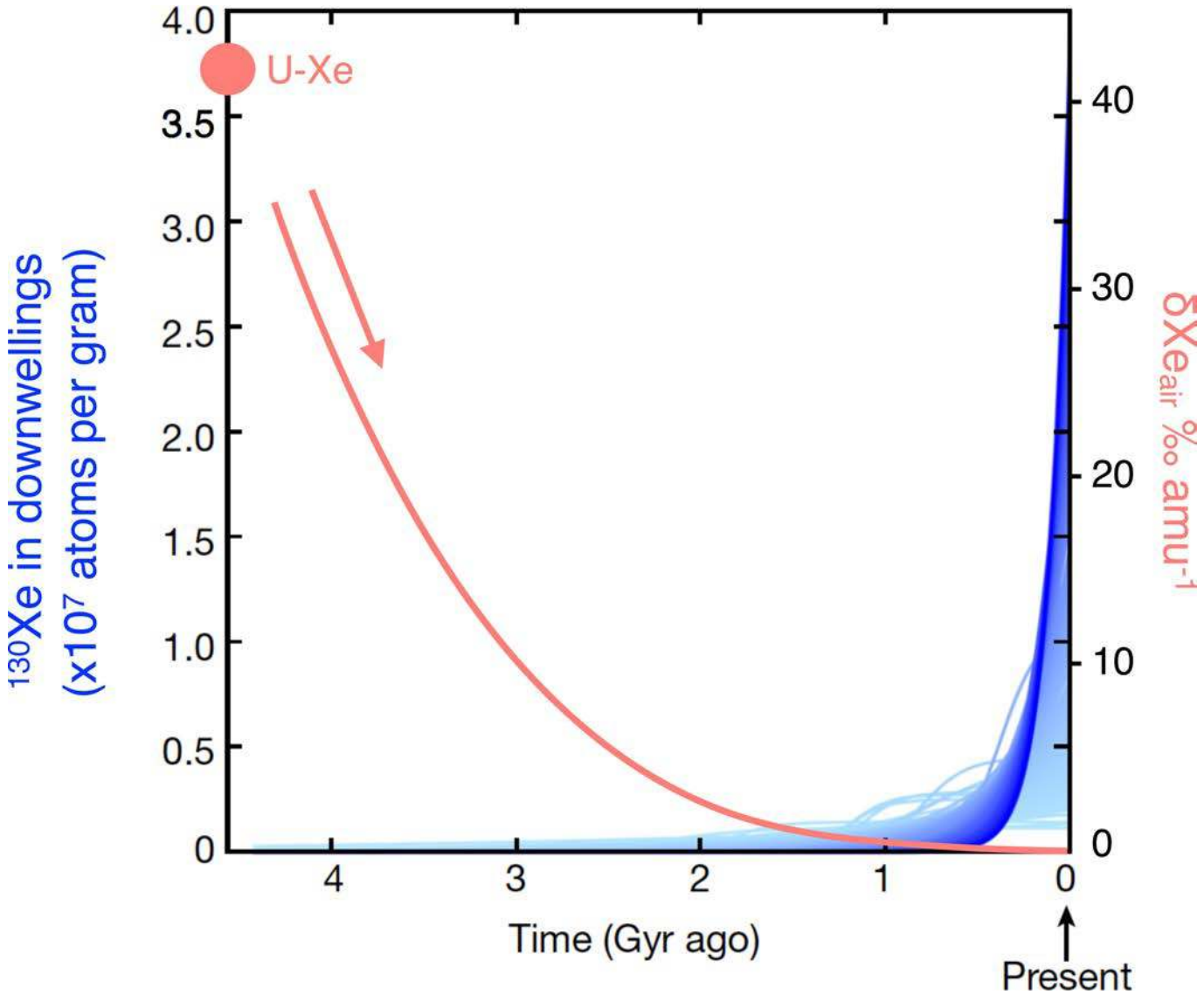

Extended Data Fig. 5 | Time series showing possible scenarios of mantle regassing histories. Shown is recycling of atmospheric Xe into the mantle (blue lines, left-hand *y* axis)[17] compared to the time evolution of atmospheric Xe isotopic composition[4] (δXe_{air}, right-hand *y* axis). The pink arrow shows the direction of atmospheric Xe isotopic evolution, from U-Xe (the progenitor of atmospheric Xe) to present. This illustrates the fact that regassing of atmospheric Xe into the mantle would have become efficient only after atmospheric Xe had reached a modern-like isotopic composition, that is, within the last 1.5 Gyr. Adapted from ref. [17].

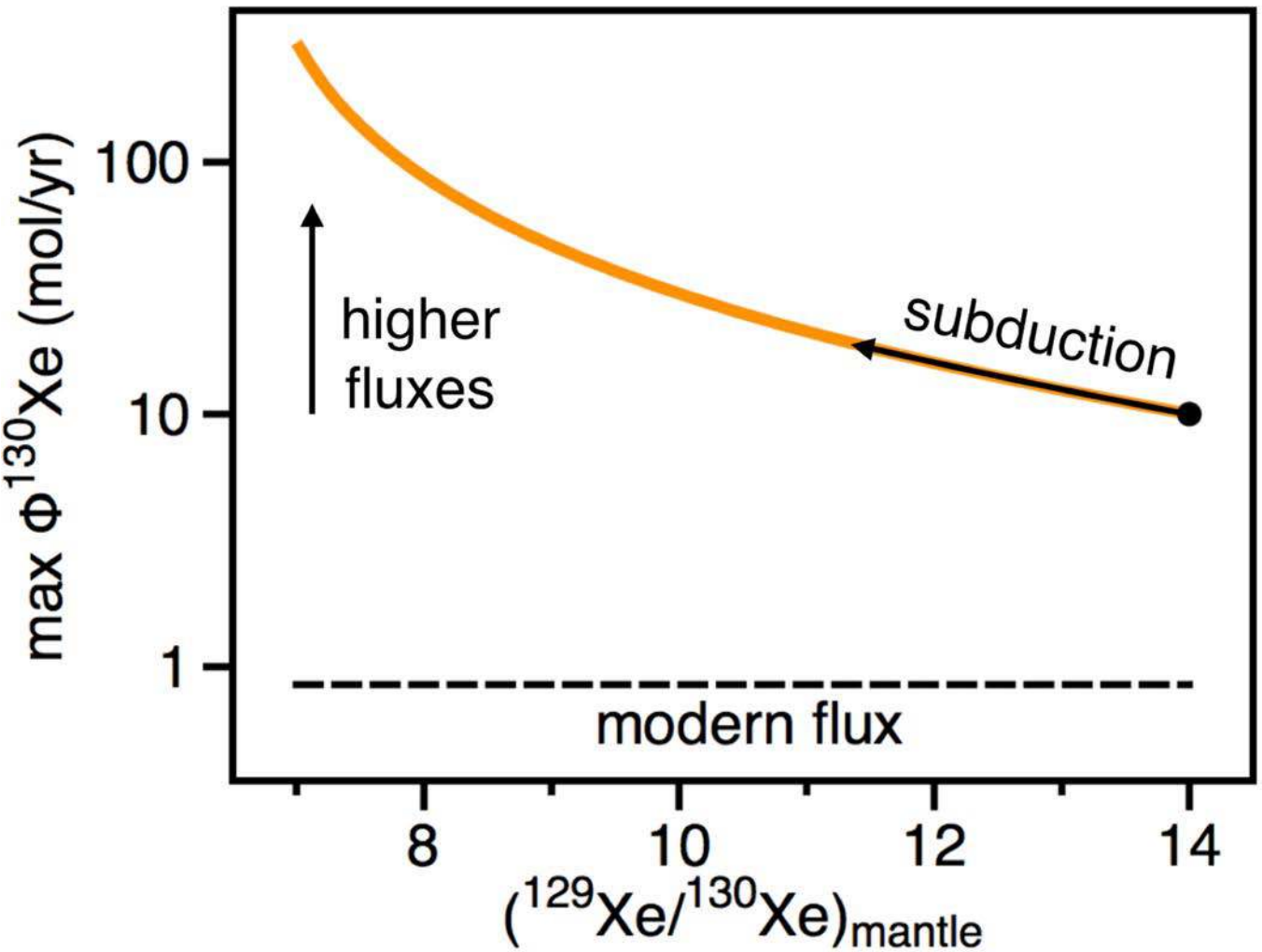

Extended Data Fig. 6 | Maximum flux of Xe (represented by ^{130}Xe) degassed from the mantle as a function of the mantle ^{129}Xe/^{130}Xe ratio. Computations reported in Fig. 2 of the main text have been carried out using a fixed mantle ^{129}Xe/^{130}Xe of 14. Here we show that lowering this ratio (for example, via subduction of atmospheric Xe) down to modern mantle-like ^{129}Xe/^{130}Xe ≈ 7–8 would result in even greater Xe fluxes from the Archaean mantle (see black arrow). Given that the onset of atmospheric Xe recycling into the mantle is not well known, possible ^{130}Xe flux values from the Archaean mantle are within the range 10–150 mol yr^{-1} (orange curve), well above the modern flux value (0.85 ± 0.35 mol yr^{-1}, horizontal dashed line; Extended Data Table 2).

Extended Data Table 1 | $\Delta^{129}Xe$ values (in ‰) versus ages (in Ga)

	Age	$\Delta^{129}Xe$	1σ	Ref.
Barberton	3.3	-6.59	1.78	8
MGTKS3#2	3.0	-5.89	2.4	4
Fortescue	2.7	-6.07	3.09	5
Vetreny	2.45	-4.44	4.86	5
Gaoua	2.1	2.63	4.38	5
Carnaiba	1.95	4.51	7.42	5
Caramal	1.7	-1.43	5.63	5
Avranches	0.5	-8.58	11.7	5
Rhynie	0.4	8.21	14	5
Recent	0.035-0	4.38	5.94	5
Barite	0.17	0.6	2	6
air	0	0		

Sample names (left column), locations, ages and original Xe data can be found in refs. [4–6,8] and at https://zenodo.org/record/3378722#.Xa6cMi3pNvE.

Extended Data Table 2 | Archaean atmospheric inventory and modern mantle flux

Atmospheric ^{129}Xe inventory			
	Value	**±**	**Refs./notes**
Atm. Xe	1.54×10^{13}	1.77×10^{11}	7
Modern atm. $^{129}Xe/^{130}Xe$	6.496	-	7
$^{129}Xe/^{130}Xe$ with 6.3±2.5 ‰ deficit	6.455	0.016	this work
$^{129}Xe_{DEF}$ deficit in the atmosphere	2.56×10^{10}	1.02×10^{10}	95% CI
Average $^{129}Xe_{XS}$ flux over 3.0 Ga	**8.5**	**3.4**	**mole/yr**
Atm. Xe lost to space			
3.5 times modern Xe inventory	8.96×10^{10}	3.57×10^{10}	95% CI
Average $^{129}Xe_{XS}$ flux over 3.0 Ga	**30**	**12**	**mole/yr**
Modern $^{129}Xe_{XS}$ flux from the mantle			
	Value	**±**	**Refs./notes**
^{3}He flux from mantle to oceans	527	102	15
^{3}He flux from subaerial volcanism	275	35	16
Global ^{3}He flux from the mantle	802	137	**mole/yr**
Mantle $^{3}He/^{130}Xe$	950	50	10
^{130}Xe flux	**0.85**	**0.32**	**mole/yr**
MORB mantle $^{129}Xe/^{130}Xe$	7.8		10,11
MORB mantle $^{129}Xe_{XS}$ flux	1.11	0.42	
Plume mantle $^{129}Xe/^{130}Xe$	7		10,11
Plume mantle $^{129}Xe_{XS}$ flux	0.44	0.17	
Modern $^{129}Xe_{XS}$ flux	**0.89**	**0.47**	**mole/yr**

Top, atmospheric inventory of missing ^{129}Xe in the Archaean atmosphere ($^{129}Xe_{DEF}$). Bottom, modern mantle $^{129}Xe_{XS}$ flux. Xe isotope fractionation in modern air indicates[5,8] specific loss of Xe from the atmosphere to space from 4.5 Ga to about 2.0 Ga. The amount of ^{129}Xe lost to space between 3.0 Ga and about 2.0 Ga is equal to 2.5 times the modern inventory (Extended Data Fig. 1). For the modern mantle $^{129}Xe_{XS}$ flux, we considered a mantle made of 1/3 plume source and 2/3 MORB source, which yields a value intermediate between those computed for either a plume composition or a MORB composition, respectively. Data are from refs.[7,10,11,15,16].

Extended Data Table 3 | Mantle and atmosphere inventories

Mantle			
	MORB source	**Plume source**	**Notes/Refs**
Modern mantle			
^{3}He mantle source	1.50×10^{-15}	1.50×10^{-13}	35
^{130}Xe/^{3}He	1.05×10^{-3}	1.05×10^{-3}	10
Mantle ^{130}Xe (mass: 4.10^{27} g)	6.32×10^{9}	6.32×10^{11}	
^{129}Xe/^{130}Xe	7.8	7.0	
Mantle Xe	1.90×10^{9}	1.76×10^{11}	
% degassed: Closed atm	97.8%	34.2%	
% degassed: Atm. escape	99.4%	64.5%	
Archean mantle			
^{3}He mantle source	1.50×10^{-15}	1.50×10^{-13}	35
^{130}Xe/^{3}He	2.11×10^{-4}	2.11×10^{-4}	10
Mantle ^{130}Xe (mass: 4.10^{27} g)	1.26×10^{9}	1.26×10^{11}	
^{129}Xe/^{130}Xe	14	14	This work
Mantle Xe	4.05×10^{10}	5.66×10^{12}	
% degassed: Closed atm	**59.1%**	**3.5%**	
% degassed: Atm escape	**67.7%**	**5.4%**	
Atmosphere			
	MORB source	**Plume source**	**Notes/Refs**
^{130}Xe/^{3}He	1.05×10^{-3}	1.05×10^{-3}	10
^{3}He/^{36}Ar	0.5	0.8	10
^{130}Xe/^{36}Ar	8.16×10^{-4}	8.16×10^{-4}	
^{40}Ar/^{36}Ar	40,000	10,000	10,11
^{40}Ar/^{36}Ar at 3 Ga	7584	1896	
^{130}Xe/^{40}Ar	1.08×10^{-7}	4.31×10^{-7}	
^{129}Xe/^{130}Xe	14	14	Pre-subduction
$^{129}Xe_{XS}$/^{40}Ar	8.07×10^{-7}	3.23×10^{-6}	
$^{129}Xe_{DEF}$	9.0×10^{10}	9.0×10^{10}	Atm. escape
^{40}Ar degassed	1.11×10^{17}	2.79×10^{16}	
^{40}Ar atm	1.65×10^{18}	1.65×10^{18}	7
% ^{40}Ar atm	**6.8%**	**1.7%**	Contrib. to atmosphere

Concentrations are given in mol g^{-1} and abundances are given in mol. Modern ^{130}Xe/^{3}He ratios for MORB and plume sources are similar within[10] 10%. Modern mantle fluxes and concentrations are from ref. [35] and noble-gas compositions are from refs. [7,10,11]. Xe contents are computed from ^{130}Xe percentage for the different Xe isotope compositions. The pre-subduction mantle composition uses extrapolated ^{129}Xe/^{130}Xe ratios (Extended Data Fig. 2 and Methods) and, for Xe abundance, is obtained by removing 80% atmospheric Xe, corresponding to atmospheric contamination that took place during the Proterozoic. The ^{40}Ar/^{36}Ar ratios at 3 Ga are corrected for ^{40}K production during the last 3 Ga.

Extended Data Table 4 | Results of models for flux evolution through time

	$^{129}Xe_{DEG}$ (moles)	φ_{max} (mole/yr)	$\%^{130}Xe_{DEG}$	
			Marty 2012	Halliday 2013
Scenario 1 (Lower limit)	2.21×10^{10}	-	1.5%	19%
Scenario 2 (Upper limit)	7.87×10^{10}	-	5.1%	45%
Scenario 3, no escape				
Power law	1.81×10^{10}	18 (3 Ga)	1.2%	16%
Exponential 1	1.56×10^{10}	25 (3 Ga)	1.1%	14%
Exponential 2	2.23×10^{10}	63 (3 Ga)	1.5%	19%
Ramp (2.6-2.2) Ga	2.23×10^{10}	56 (2.6 Ga)	1.5%	19%
Ramp (2.5-2.4) Ga	2.23×10^{10}	224 (2.5 Ga)	1.5%	19%
Scenario 3 with escape				
Power law	3.98×10^{10}	64 (3 Ga)	2.7%	29%
Exponential 1	3.77×10^{10}	89 (3 Ga)	2.5%	28%
Exponential 2	6.10×10^{10}	220 (3 Ga)	4.0%	39%
Ramp (2.6-2.2) Ga	4.85×10^{10}	141 (2.6 Ga)	3.2%	34%
Ramp (2.5-2.4) Ga	5.02×10^{10}	519 (2.5 Ga)	3.3%	34%

See Methods for definition of scenarios. $^{129}Xe_{DEG}$ corresponds to integrated amounts (in mol) of ^{129}Xe required to have been degassed from the mantle to account for the isotopic evolution of atmospheric Xe. Φ_{max} are the maximal fluxes of mantle ^{129}Xe. $^{130}Xe_{DEG}$ (%) corresponds to the fraction of the mantle ^{130}Xe inventory required to have been degassed, for mantle budget estimates by Marty[42] and Halliday[36], and for a mantle $^{129}Xe/^{130}Xe$ of 14.